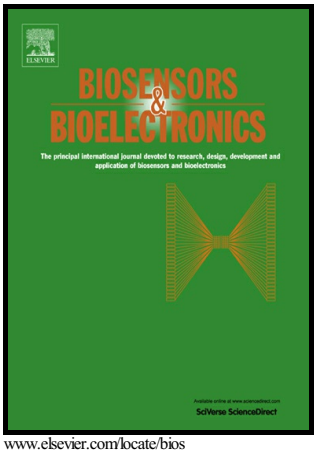

www.elsevier.com/locate/bios

Target triggered cleavage effect of DNAzyme: Relying on Pd-Pt alloys functionalized Fe-MOFs for amplified detection of Pb^{2+}

Yujie Yu, Chao Yu, Yazhen Niu, Jun Chen, Yilin Zhao, Yuchan Zhang, Rufei Gao, Junlin He

PII: S0956-5663(17)30666-8
DOI: https://doi.org/10.1016/j.bios.2017.10.006
Reference: BIOS10031

To appear in: *Biosensors and Bioelectronic*

Received date: 20 July 2017
Revised date: 15 September 2017
Accepted date: 2 October 2017

Cite this article as: Yujie Yu, Chao Yu, Yazhen Niu, Jun Chen, Yilin Zhao, Yuchan Zhang, Rufei Gao and Junlin He, Target triggered cleavage effect of DNAzyme: Relying on Pd-Pt alloys functionalized Fe-MOFs for amplified detection of Pb^{2+}, *Biosensors and Bioelectronic,* https://doi.org/10.1016/j.bios.2017.10.006

Target triggered cleavage effect of DNAzyme: Relying on Pd-Pt alloys functionalized Fe-MOFs for amplified detection of Pb^{2+}

Yujie Yu[1], Chao Yu[1], Yazhen Niu, Jun Chen, Yilin Zhao, Yuchan Zhang, Rufei Gao, Junlin He [*]

School of Public Health and Management, College of Pharmacy, Chongqing Medical University, Chongqing 400016, PR China

*Corresponding author: Prof. Junlin He. Full address: Box 380#, College of Pharmacy, Chongqing Medical University, 1 Yi Xue Yuan Road, Chongqing 400016, P. R. China. Phone: (86) 23-68485378. Fax: (86) 23-68485161. hejunlin_11@aliyun.com

ABSTRACT

We designed an amplified detection strategy for the sensitive determination of lead ions (Pb^{2+}) based on a target-triggered nuclear acid cleavage of Pb^{2+}-specific DNAzyme as a selectivity interface combined with Pd-Pt alloys modified Fe-MOFs (Fe-MOFs/PdPt NPs) hybrids acting as the signal tag. Streptavidin modified reduced graphene oxide-tetraethylene pentamine-gold nanoparticles (rGO-TEPA-Au) served as a sensor platform for immobilizing more DNAzyme. In the presence of Pb^{2+}, the substrate DNA strand can be specifically cleaved at the ribonucleotide site by DNAzyme to produce a new single-DNA on the interface. Then, the hairpin DNA with hybrid strand matched by its complement to the single-DNA was employed to modify the Fe-MOFs/PdPt NPs bioconjugates for signal amplification. Fe-MOFs/PdPt NPs catalyze hydrogen peroxide (H_2O_2) to produce the electrochemical signal which was recorded by chronoamperometry. Benefiting from the Pb^{2+}-dependent DNAzyme, the proposed method can selectively detect Pb^{2+} in the presence of other metal ions. The newly designed biosensor exhibited a good linear relationship ranging from 0.005 to 1000 nmol L^{-1} with a low detection limit of 2 pM (S/N=3) for Pb^{2+}. This Pb^{2+}-dependent DNAzyme based ultrasensitive biosensor showed high sensitivity and

[1] Chao Yu and Yujie Yu contributed equally to this work.

selectivity, providing potential application for Pb^{2+} detection in naturally contaminated sewage and spiked drinking water samples.

Keywords: Pb^{2+} detection; Pb^{2+}-dependent DNAzyme; Fe-MOFs/PdPt NPs; Ultrasensitive

1. Introduction

Long-term exposure or excessive intake of lead ions (Pb^{2+}) can cause neurological, cardio-vascular, reproductive, and developmental disorders (Fan et al.,2008; Huang et al.,2008; Marbella et al.,2009). Monitoring the levels of Pb^{2+}, especially the trace amounts of lead in the environment and food industry, has become an important issue (Vodyanitskii et al., 2013). Atomic absorption spectrometry (AAS), atomic fluorescence spectrometry, and inductively coupled plasma mass spectrometry (ICP-MS) are the traditional techniques utilized for Pb^{2+} determination (Calvo Quintana et al.,2012; Liang and Sang,2008; Zhang et al.,2016). While these methods are sufficiently sensitive, they also quite complicated. Thus, it is necessary to develop a rapid, convenient and highly sensitive method for Pb^{2+} analysis. To date, electrochemical techniques have been widely applied owing to their advantages of wide dynamic concentration response range, remarkable sensitivity, spatial controllability, cost-effective and simple preprocessing (Ge et al.,2014; Tang et al.,2008). Therefore, we design an amplified detection strategy for the detection of Pb^{2+} ions in aqueous solutions.

The 8-17 DNAzyme, a kind of active DNA molecule containing the catalytic core motif as 8-17 deoxynucleotides, is a RNA-cleaving enzyme consisting of a substrate strand and a catalytic strand and has a specific cleavage site in the presence of Pb^{2+} (Santoro and Joyce,1998). Relying on the Pb^{2+}-dependent catalytic activity to cleave the substrate to two pieces of strands, it has been used for Pb^{2+} detection based on different signal-production principles (Hung et al.,2010; Li et al.,2010; Tang et al.,2013; Xu et al.,2013). In the presence of Pb^{2+}, the substrate strand of the

DNAzyme catalytically cleaved by target and a new single-strand DNA was produced. The signal tag matched by the new single-strand DNA, which can be used as the post-amplification strategy for the detection of Pb^{2+}, such as a single-stranded DNAzyme-based Pb^{2+} fluorescent sensor (Shen et al.,2008). Therefore, based on the post-amplification strategy, the development of a new signal amplification strategy for the sensitive and selective detection of Pb^{2+} is highly desirable.

To increase the sensitivity of the biosensor, considerable efforts have been devoted to immobilize the 8-17 DNAzyme and amplify the signals (Yuan et al.,2015). Reduced graphene oxide-tetraethylene pentamine (rGO-TEPA) is a desirable material that contains many amino groups, making it an ideal template for loading gold nanoparticles (AuNPs) to further enhance its performance further. Since the nanocomposite rGO-TEPA-Au can be immobilized with streptavidin through the Au-NH_2 covalent bonds, it is easier for the biotin-modified substrate strand of 8-17 DNAzyme to support on the surface of the biosensor via the biotin-streptavidin system (Lee et al.,2008). Furthermore, for the signal amplification, palladium-platinum (Pd-Pt) alloys modified Fe-MIL-88 metal-organic framework (Fe-MOFs/PdPt NPs) hybrids were introduced. MOFs, a new type of host matrix material, have attracted considerable attention for their high specific surface areas, tunable pore sizes and exposed active sites (Carne et al.,2011). Specially, Fe-MOFs exhibit highly peroxidase-like activity. Moreover, bimetallic alloys are of particular importance in catalysis because the addition of the second metal provides variations in chemical and physical properties consisting of catalytic activity and chemical selectivity. Specifically, Pt-based bimetallic systems have proved themselves as novel architectures with significantly improved catalytic and electrocatalytic activity (Chen et al.,2012). Therefore, Pd-Pt alloys are a promising candidate of fabrication biosensors because the synergistic effect of Pd and Pt enhance the performance of the resultant electrodes by the catalysis of hydrogen peroxide (H_2O_2) (Chen et al.,2012). In this regard, Pd–Pt alloys in combination with Fe-MOFs to produce and amplify the signal. Additionally, Fe-MOFs/PdPt NPs combined with the mercapto group labeled hairpin DNA (HP) that can match with the newly generated single-strand DNA, which

was utilized as the signal tag in this signal amplification strategy for the detection of Pb^{2+}.

Herein, we designed a highly sensitive and selective biosensor for the detection of Pb^{2+} by immobilizing Pb^{2+}-dependent DNAzyme onto a streptavidin-functionalized rGO-TEPA-Au platform. In the presence of Pb^{2+}, the substrate strand of the DNAzyme is catalytically cleaved by the target, resulting in the detachment of catalytic strand from the sensor. The newly generated single-strand DNA on the sensor can hybridize with the hairpin DNA, labeled with Fe-MOFs/PdPt NPs. The applification of Pb^{2+}-dependent DNAzyme strengthened the selectivity of the biosensor, whilst utilization of Fe-MOFs/PdPt NPs-HP catalyze H_2O_2 to amplify the electrochemical signal and enhanced the sensitivity for the first time. Furthermore, the biosensor was applied to the detection of Pb^{2+} in water samples, which showed excellent analytical performance for Pb^{2+}, indicating its great potential for applications in environment monitoring.

2.Experimental

2.1. Materials and chemicals

Reduced Graphene Oxide TEPA (rGO-TEPA) was provided by Nanjing XFNANO Materials TECH Co., Ltd. (Nanjing, China). Gold (III) chloride trihydrate ($HAuCl_4{\cdot}4H_2O$), chloroplatinic acid ($H_2PtCl_6{\cdot}6H_2O$), streptavidin, sodium tetrachloropalladate (II) (Na_2PdCl_4), dimethylformamide (DMF) and tris (2-carboxyethy) phosphine hydrochloride (TCEP) were obtained from Sigma-Aldrich (St. Louis, USA, www.sigmaaldrich.com). Potassium ferricyanide ($K_3Fe(CN)_6$) and potassium ferrocyanide ($K_4Fe(CN)_6$) were obtained from Beijing Chemical Reagents Company (Beijing,China). $NaBH_4$, H_2O_2, $FeCl_3{\cdot}6H_2O$ and acetic acid were purchased from Chongqing Chuandong Chemical Group Co., Ltd. (Chongqing, China). Leadacetate trihydrate ($Pb(OAc)_2{\cdot}3H_2O$) and bovine serum albumin (BSA) were received from Aladdin (China, www.aladdin-e.com). DNA oligonucleotides and PVP were purchased from Sangon Biotech Co., Ltd. (Shanghai, China).

The DNA oligonucleotide sequences for this experiment were listed as follows:

Substrate strand: 5'-bio-CGATAACTCACTATraGGAAGAGATG-3'

Catalytic strand: 5'-CATCTCTTCTCCGAGCCGGTCGAAATAGTGAGT-3'

Complementary DNA: 5'-SH-TTTGCCTGCATAGTGAGTATCGGCAGGC-3'

The buffer solutions involved in this study were as follows: 1×TAE buffer (40 mM Tris-acetate and 1 mM EDTA，pH 8.0), used to dissolve the substrate strand and catalytic strand. The hybridization buffer (40 mM Tris-acetate, 10 mM TCEP, 1 mM EDTA, and 3.0 mM Mg^{2+}, PH 7.4) was used to diluted the complementary DNA and signal probe. All other reagents were of analytical reagent grade and were used without further purification. Ultrapure water (>18.2 MΩ.cm) obtained from a Millipore Mill-Q purification system was used throughout the experiment.

2.2. Apparatus and characterization

All electrochemical experiments were carried out using a CHI 660E workstation at room temperature with a three-electrode system consisting of a saturated calomel electrode (SCE) as the reference electrode, a platinum wire electrode as the counter electrode, and a modified glassy carbon electrode (GCE, 4 mm in diameter) as the working electrode. The morphologies of the materials were characterized using X-ray diffraction (XRD, Y-2000, Dandong oron ray instrument co., Ltd, China) and transmission electron microscopy (TEM, Hitachi-7500158, Japan). Field emission scanning electron microscopy (FE-SEM) and Energy dispersive X-ray spectroscopy (EDS) images were collected using a JEOLJSM-6700F microscope. X-ray photoelectron spectroscopy (XPS) was performed using a VG Scientic ESCALAB 250 spectrometer (Thermo Nicolet, USA). Atomic force microscopy (AFM) images were obtained using a Bruker Dimension icon instrument (USA).

2.3. Preparation of rGO-TEPA-Au

The rGO-TEPA-Au was synthesized according to the previous work with slight modification (Yu et al., 2016). Briefly, 2 mg of rGO-TEPA was dispersed into 1 mL of

ultrapure water and sonicated for 1 h. Then, the obtained dispersion was mixed with 1.45 mL of 0.8 M AA, 0.5 mL of 2.0 M PVP, 1 mL of 2% $HAuCl_4$, and then heated to 90°C in vigorous magnetic stirring for 3 h. Finally, the products were purified by centrifugation and washing with ultrapure water, and the resultant rGO-TEPA-Au was dispersed in 1 mL of ultrapure water for further use.

2.4. Preparation of Fe-MOFs and Fe-MOFs/PdPt NPs, Fe-MOFs/AuNPs, Fe-MOFs/PtNPs, Fe-MOFs/PdNPs

Fe-MIL-88 MOFs were synthesized according to the literature with certain modifications (Xie et al.,2015). Fe-MOFs/PdPt NPs were prepared as follows. Briefly, 0.692 mM (0.126 g) of 2-aminoterephthalic acid and 0.692 mM (0.187 g) of $FeCl_3{\cdot}6H_2O$ were dispersed in 15 mL of DMF. The obtained solution was heated in a silicone oil bath at 120°C for 15 min, followed by the injection of 3.45 mM acetic acid and continued heating for 4 h. After slowly cooling to room temperature, the resultant Fe-MIL-88 MOFs were isolated by centrifugation and successively washed with DMF, ethanol and ultrapure water. Finally, the products were dried in a vacuum overnight. The detailed procedures for the syntheses of the Fe-MOFs/AuNPs, Fe-MOFs/PtNPs, and Fe-MOFs/PdNPs nanocomposite are provided in the Supplementary Information (S1). The synthesis procedure of Fe-MOFs/PdPt NPs was performed as follows. Briefly, 0.5 mL of H_2PtCl_6 (1%) and 0.5 mL of Na_2PdCl_4 (1%) was added to 1 mL of Fe-MOFs solution (1 mg mL^{-1}) and vigorously sonicated for 20 min. Then 2 mL of a $NaBH_4$ (0.1 M) solution was added dropwise into the complex solution with stirring at 400 rpm for 30 min. Subsequently, the mixture was purified by centrifugation and washing with ultrapure water three times, followed by dispersal in 1 mL of ultrapure water for further use.

2.5. Preparation of the Fe-MOFs/PdPt NPs-HP-BSA

Briefly, 2 μM of complementary DNA, labeled at the 5'-SH, was heated at 95℃ for 5 min. Then, the solution was slowly cooled to room temperature to form

stem-loop structures for at least 2 h. Subsequently, 200 μL of thiol-terminated HP (2 μM) was added into 1 mL of a prepared Fe-MOFs/PdPt NPs solution under gentle stirring for 12 h at 4℃. To block nonspecific adsorption sites, BSA was added to the above solution. After centrifugation at 8000 rpm for 5 min and washing three times with ultrapure water, the Fe-MOFs/PdPt NPs-HP-BSA were obtained, and were dispersed in 1mL of hybridization buffer (pH 7.4) and stored at 4℃ when not in use.

2.6. Fabrication of electrochemical biosensor

The fabrication process of the biosensor is schematically illustrated in Scheme 1. Prior to the modification, GCE was polished with alumina slurries of 0.3 and 0.05 μm followed by sonication in ultrapure water, ethanol and ultrapure water. Subsequently, the electrode was dried in air and modified with 10 μL of the rGO-TEPA-Au nanocomposite. After drying at room temperature, 10 μL of streptavidin solution (100 μg mL^{-1}) was added onto the modified electrode at 4℃ for 12 h. During this process, the streptavidin was immobilized on the electrode via Au-NH_2 bonding. Then, the electrode was washed with ultrapure water to remove excess reagents and was dried in air. Afterward, 10 μL of the biotin modified substrate strand (1 μM) was immobilized onto the prepared electrode for 45 min at 4℃. Next, the prepared electrode was washed with ultrapure water followed by blocking with a BSA solution (1%, w/v) for 30 min at room temperature to prevent nonspecific adsorption. Subsequently, the modified electrode was incubated with 10 μL of catalytic strand (1 μM) for 2 h at 37℃ to form the Pb^{2+}-specific DNAzyme. Then, different concentrations of Pb^{2+} were dropped onto the prepared electrode and reacted for 45 min at 37℃. In the presence of Pb^{2+}, the DNAzyme was activated, and the substrate strand was cleaved. After washing again, 10 μL of the synthesized Fe-MOFs/PdPt NPs-HP-BSA bioconjugates were coated onto the as-prepared electrode for 2 h to realize the signal amplification. After hybridization, the electrode was rinsed with ultrapure water and prepared for electrochemical analysis.

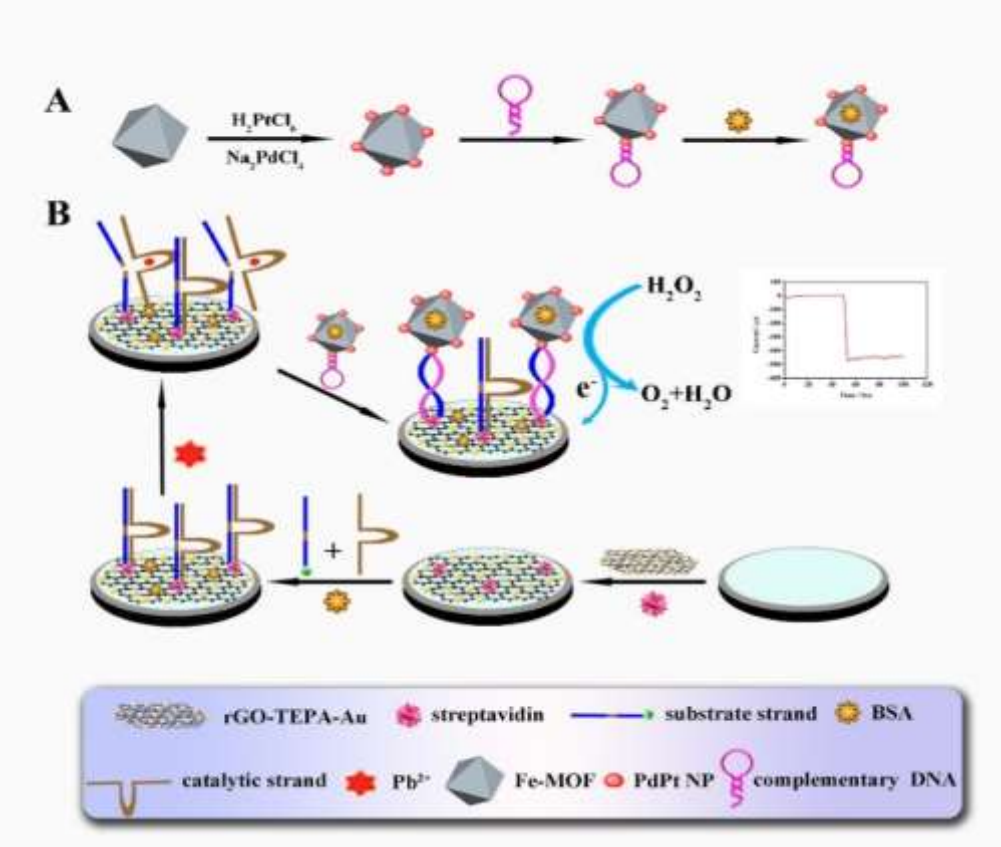

Scheme 1. (A) Preparation process of Fe-MOFs/PdPt NPs-HP. (B) Schematic representation of the proposed strategy for the biosensor.

2.7. Electrochemical detection

Electrochemical detection of amperometric i-t curves was recorded at 0.4 V in 5 mL of phosphate buffered saline (PBS) (pH 7.4) at room temperature. After the background current was stable, 20 μL of H_2O_2 (1.8 mol L^{-1}) was added into the solution, and the current changes were recorded.

3. Results and discussion

3.1. Characterization of different nanomaterials.

FE-SEM and TEM were used to investigate the morphology and structure of the as-prepared materials. As shown in Fig. 1A and Fig. S1A, the rGO-TEPA exhibited smooth and continuous surface with some crumpled morphologies. After the rGO-TEPA was modified with AuNPs by in situ reduction of $HAuCl_4$, it can be seen

that the AuNPs were uniformly distributed on the surface of rGO-TEPA sheets (Fig. 1B, Fig. S1B), suggesting the successful synthesis of rGO-TEPA-Au. Additionally, Fig. 1C and Fig. S1C shows that the Fe-MIL-88 MOFs exhibited regular octahedron structures with a size of approximately 100 nm, which was consistent with the previous report (Liu et al.,2013). After the Fe-MOFs were functionalized with PdPt NPs, the Fe-MOFs were coated with amounts of spherical particles (Fig. 1D, Fig. S1D), indicating that Fe-MOFs/PdPt NPs were successfully synthesized.

To further demonstrate the successful synthesis of rGO-TEPA-Au and Fe-MOFs/PdPt NPs nanocomposites. EDS and XPS were used for element analysis. As shown in Fig. 1E, the significant peaks for C, N, O and Au were obtained in the EDS image. Furthermore, the characteristic peaks for the Au4f, C1s, N1s, and O1s core level regions were clearly obtained in the rGO-TEPA-Au composites from the XPS image (Fig. 1F), suggesting the successful synthesis of rGO-TEPA-Au. The EDS and XPS images of Fe-MOFs/PdPt NPs nanocomposites are displayed in Fig. 1G and 1H. The significant peaks of C, N, O, Fe, Pt and Pd in the EDS image and the characteristic peaks for the Pt4f, C1s, Pd3d, O1s and Fe2p in the XPS image revealed that Fe-MOFs/PdPt NPs were successfully synthesized. Moreover, TEM and XRD were used to indicate the successful synthesis of rGO-TEPA-Au and Fe-MOFs/PdPt NPs nanocomposites. The results were shown in the Supplementary Information (Fig S1, Fig. S2).

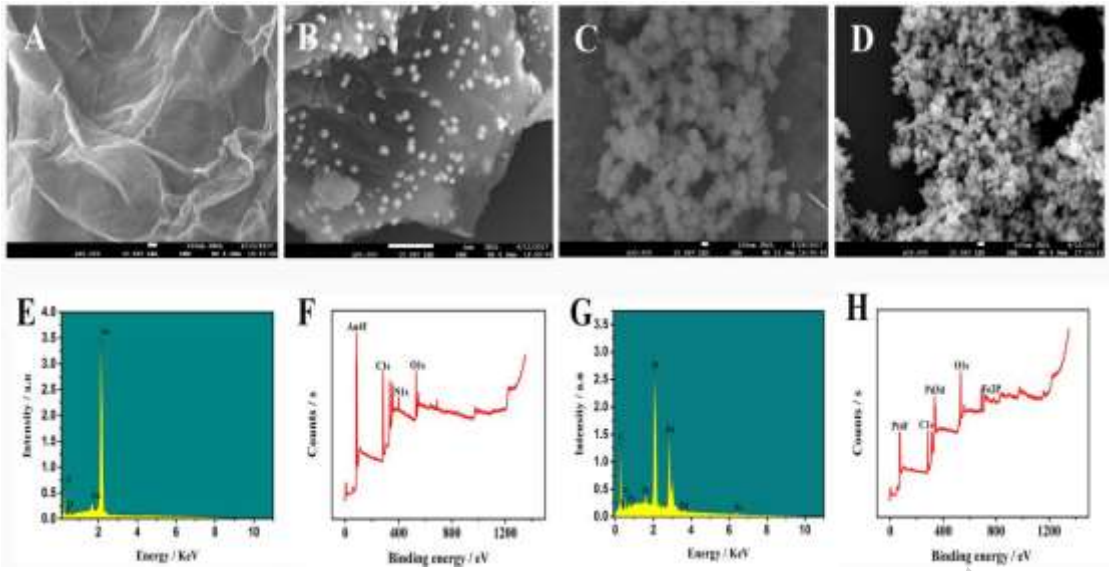

Fig. 1. FE-SEM images of rGO-TEPA (A), rGO-TEPA-Au (B), Fe-MIL-88 MOFs (C) and Fe-MOFs/PdPt NPs (D). EDS images of rGO-TEPA-Au (E) and Fe-MOFs/PdPt NPs (G). The XPS spectra of rGO-TEPA-Au (F) and Fe-MOFs/PdPt NPs (H)

3.2. The electrochemical behaviour of different nanomaterials for signal tags

The amperometric i-t curve was employed to compare the electrochemical behaviours of different naonomaterials. As shown in Fig.2A, curve a showed the i-t responses of Fe-MOFs, which indicated that Fe-MOFs have a weak catalytic ability towards H_2O_2. After AuNPs were reduced on the Fe-MOFs, the Fe-MOFs/AuNPs nanocomposite (curve b) showed an enhanced catalysis current compared to that of Fe-MOFs because AuNPs can catalyze H_2O_2 (Luo et al., 2014). Owing to the stronger catalytic ability of PtNPs relative to that of AuNPs (Liu et al.,2014), the electrochemical signal increased (curve c) when PtNPs were immobilized onto the Fe-MOFs. The electrochemical signal further increased (curve d) when PdNPs were modified onto the Fe-MOFs. Finally, when the Fe-MOFs were functionalized with PdPt NPs, the catalytic ability was obviously increased (curve e) owing to the synergistic catalytic activities of PdPt NPs. The results demonstrated that our proposed nanocomposite had an excellent catalytic ability, which can significantly improve the detection sensitivity.

3.3. Characterization of stepwise fabrication of the biosensor

Cyclic voltammetry (CV) measurement was used to investigate the assembly steps of the sensing interface. The CVs of different modified electrodes were monitored in a 5 mM $[Fe(CN)_6]^{3-/4-}$ solution. As shown in Fig.2B, a pair of redox peaks can be observed on the bare GCE (curve a). When rGO-TEPA-Au was cast onto the bare GCE, the oxidation and reduction peak currents increased obviously (curve b). Because the rGO-TEPA possessed excellent electrical conductivity, and the AuNPs can enhance the electron transfer. After the streptavidin was immobilized onto the modified electrode, a drastic decrease in the peak current was observed (curve c) owing to the poor conductivity of streptavidin. When the resultant electrode was incubated with the substrate strand, the peak current decreased apparently (curve d) because of the resistance of $[Fe(CN)_6]^{3-/4-}$ from approaching the electrode by the abundant negatively charged DNA backbones. Non-conductive BSA, as a blocking agent, caused another decrease of the peak current (curve e). Moreover, the redox peak currents further decreased after the electrode was incubated with the catalytic strand, because the catalytic strand can hinder the electron transfer towards the electrode surface (curve f) due to their non-electroactive property. After the resultant electrode was immobilized with Pb^{2+}, the redox peak current increased (curve g), indicating that Pb^{2+}-dependent DNAzyme cleaved its substrate. Since the negatively charged DNA backbones decreased, the electron transfer can be accelerated.

As an effective tool for characterizing the modified electrode, electrochemical impedance spectroscopy (EIS) was also utilized to validate the fabrication process. In the Nyquist diagram, the electron-transfer resistance is equal to the semicircle diameter, and the linear portion at lower frequencies represent the diffusion process. As shown in Fig. 2C, the bare GCE presented a small semicircle (curve a). After rGO-TEPA-Au was coated onto the electrode surface, the resistance decreased (curve b) owing to the accelerated electron transfer caused by rGO-TEPA-Au. Compared to curve b, a gradual increase in resistance was observed (curve c), which was attributed to the presence of streptavidin that can hinder the electron transfer. When the modified electrode was incubated with the substrate strand, the semicircle diameter increased (curve d) because of the resistance of $[Fe(CN)_6]^{3-/4-}$ from approaching the

electrode by the negatively charged DNA backbones. After blocking with BSA, the resistance further increased (curve e) because BSA hindered the electron transfer. Subsequently, the semicircle diameter increased (curve f) when the resultant electrode was immobilized with the catalytic strand, because more negatively charged DNA backbones were obtained. Finally, the semicircle diameter decreased (curve g), which was ascribed to the fact that the Pb^{2+}-dependent DNAzyme cleaved its substrate in the presence of Pb^{2+}. Meanwhile, AFM is a useful approach to characterize the interface properties of electrodes. A detailed description can be found in the Supplementary Information (Fig. S3). All these results confirmed the successful fabrication of the biosensor.

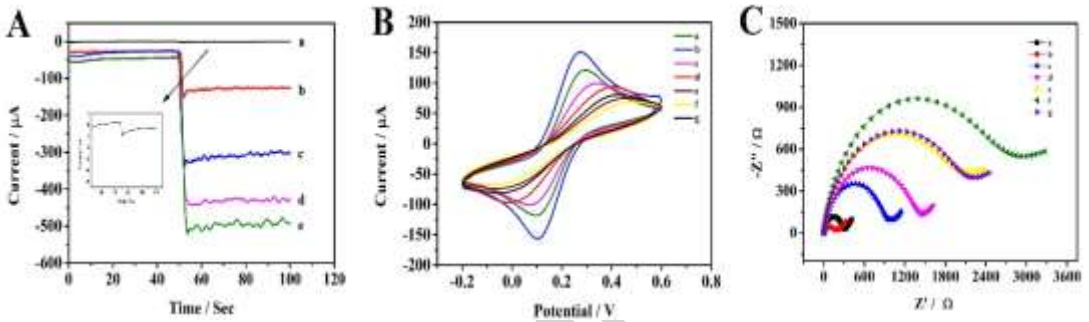

Fig. 2. (A) The Amperometric i-t curves of different nanomaterials: (a) Fe-MOFs, (b) Fe-MOFs/AuNPs, (c) Fe-MOFs/PtNPs, (d) Fe-MOFs/PdNPs, (e) Fe-MOFs/PdPt NPs; (B) CV and (C) EIS characterization of electrodes at various stages of modification in a 5 mM $[Fe(CN)_6]^{3-/4-}$ solution: (a) bare GCE, (b) rGO-TEPA-Au/GCE, (c) streptavidin/rGO-TEPA-Au/GCE, (d)substrate strand/streptavidin/rGO-TEPA-Au/GCE, (e) BSA/substrate strand/streptavidin/rGO-TEPA-Au/GCE, (f) catalytic strand/BSA/substrate strand/streptavidin/rGO-TEPA-Au/GCE, (g) Pb^{2+}/catalytic strand/BSA/substrate strand/streptavidin/rGO-TEPA-Au/GCE.

3.4. Optimization of the experiment conditions

A series of experiments were employed to optimize the conditions with the acceptable signal response. The effect of the volume of rGO-TEPA, the concentration of streptavidin and the substrate strand, the influence of the immobilization time of the substrate strand, the hybridization time between the substrate strand and the catalytic strand, and the concentration of H_2O_2 were investigated.

The volume of rGO-TEPA was a key factor that influences the surface area of the electrode and can improve the sensitivity of the biosensor. The volume of rGO-TEPA was tested in the range from 4 to 14 μL. The results in Fig. S2A suggested that the changes increased until a volume of 10 μL, and then began to level off. Therefore, the optimal formation volume of rGO-TEPA was determined to be 10 μL.

The concentration of streptavidin played an important role in immobilizing the substrate strand and biosensor performance. The concentration of streptavidin was tested in the range from 40 to 140 μg mL^{-1}. As shown in Fig. S2B, the current change increased from 40 μg mL^{-1} to 100 μg mL^{-1}. A further increase of the concentration of streptavidin had no remarkable effect on the current change. Therefore, 100 μg mL^{-1} was selected as the optimal concentration of streptavidin.

Furthermore, the concentration of the substrate strand and the immobilized time of the substrate strand were also optimized. As shown in Fig. S2C, the current change increased with the increasing concentration of the substrate strand from 0.5 to 1.0 μM and then maintained a steady state. Thus, 1.0 μM was selected as the optimum concentration of the substrate strand. In addition, as the time increased to 45 min, the current change trended to a plateau because the immobilization of substrate strand was almost completed when the time was 45 min (Fig. S2D). Therefore, the optimal immobilized time of substrate strand was chosen as 45 min.

For recognition of Pb^{2+}, the hybridization time is a notably important parameter. The results in Fig. S2E shows that the current change increased from 1.0 to 2.0 h. When the hybridization time was greater than 2.0 h, the current changes remained stable. Therefore, 2.0 h was selected as the optimal hybridization time.

To achieve the optimal electrochemical signal, the concentration of H_2O_2 was investigated. As shown in Fig. S2F, the current response increased from 1.0 to 1.8 mol L^{-1} and then reached saturation. Therefore, 1.8 mol L^{-1} of H_2O_2 was chosen throughout the detection process.

3.5. Analytical performance of the biosensor

Under the optimized assay conditions, the sensitivity of the biosensor for the detection of the Pb^{2+} was investigated by varying the Pb^{2+} concentrations. It was obviously obtained that the electrochemical signal increased with the increase of Pb^{2+} concentrations (Fig. 3A). The plot of the current signal change vs. the logarithm of Pb^{2+} concentration showed a linear relationship in the detection range from 0.005 to 1000 nM, with the detection limit of 2 pM at the signal to noise ratio of 3 (inset in Fig. 3B). The regression equation was $Y=22.164*\log C_{Pb}^{2+}+311.83$ ($R^2=0.9993$), where Y is an amperometric i-t current increment, C_{Pb}^{2+} is the concentration of Pb^{2+}, and R^2 is the regression coefficient. Furthermore, the linear range and detection limit of the biosensor were compared with those for the previously reported methods in Table S2. The linear range and detection limit are superior to other methods, illustrating that the fabricated biosensor exhibited a higher sensitivity.

3.6. Specificity, stability and reproducibility of the DNA biosensor

Previous studies have demonstrated that the specific DNAzyme for the pairing of Pb^{2+} shows high specificity in distinguishing the target Pb^{2+} from other metal ions. The effects of interfering ions (Zn^{2+}, Bi^{3+}, Ca^{2+}, Co^{2+}, Mg^{2+}, Cu^{2+}), the mixture (Mix) (consisted of the 1.0 μM interference ions and 10 nM Pb^{2+}), and zero analyte on the biosensor were investigated, respectively. As shown in Fig. 3C, in contrast to the blank assay, it was observed that the current response did not remarkably increase with the addition of a number of ions at a concentration which was 100-fold of the Pb^{2+} concentration. The current response of Mix had no significant difference with that caused by Pb^{2+}. These results showed that the proposed sensor displays high selectivity.

The biosensor was stored at 4℃. After storage for 28 days, the change in the current remained 86.0% of its original current change (Fig. S3). The results indicated that the proposed sensor shows good stability. To evaluate the reproducibility of the proposed biosensor, the biosensor was investigated by monitoring the current signal in the presence of 1.0 μM Pb^{2+} for five replicate determinations under the same

conditions（Fig. 3D). The relative standard deviation (RSD) of the proposed sensor was found to be 3.27%, demonstrating its good reproducibility.

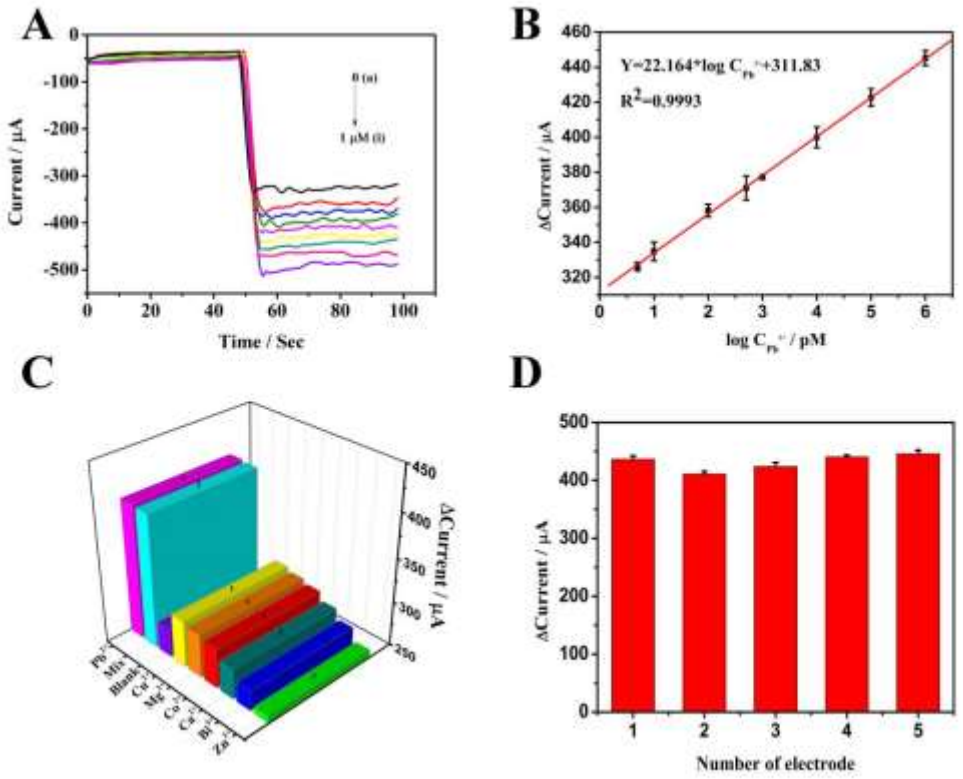

Fig. 3. (A) The i-t curve signals of the biosensor for the determination of different concentrations of Pb^{2+}: (a) 0 pM, (b) 5 pM, (c) 10 pM, (d) 100 pM, (e) 500 pM, (f) 1 nM, (g) 10 nM, (h) 100 nM, (i) 1000 nM. (B) The calibration curve of the biosensor for different concentrations of Pb^{2+} (n=3). (C) Selectivity of the biosensor for Pb^{2+}(10.0 nM), several competing 6 interfering metal ions (Zn^{2+}, Bi^{3+}, Ca^{2+}, Co^{2+}, Mg^{2+}, Cu^{2+}) (1.0 μM), a mixture (Mix) of the interference metal ions (1.0 μM) and Pb^{2+}(10.0 nM) and zero analyte (Blank). (D) Reproducibility of five different electrodes modified with 1.0 μM of Pb^{2+}.

3.7. Analytical application of the biosensor in real samples

3.7.1. Detection performance in water samples

To examine the feasibility of the biosensor for the detection of authentic samples, the biosensor was applied to water samples spiked with 1 nM, 500 nM, and 1000 nM Pb^{2+} (Table S1), and the recoveries of the three concentrations were 96.00%, 102.31%, and 97.75%, and RSDs of the three concentrations were 0.15%, 0.11%, and 0.27%,

respectively, suggesting acceptable precision.

3.7.2. Detection of Pb^{2+} in real samples

In view of the fact that the prepared biosensor had excellent sensitivity and selectivity for Pb^{2+} in real samples. The method in this work was applied for real samples such as reservoir water (N1-N3, W1-W3), well water (W4-W6) and tap water (W7). And the results are shown in Table 1. Examination of the data in Table 1 shows that this method can be reasonably applied in the environmental detection of Pb^{2+}.

Table 1 Detection of Pb^{2+} in real samples with the proposed biosensor

Sample	Sample number	Atomic absorption spectrophotometer (nM)	Present work ($\bar{x}$, nM)	Error
Reservoir water1	N1	–	–	–
	N2	–	–	–
	N3	–	–	–
Reservoir water2	W1	24.70	24.55	-0.15
	W2	2.82	2.76	-0.06
	W3	6.18	6.06	-0.12
Well water	W4	9.35	9.37	0.02
	W5	12.46	13.15	0.69
	W6	18.69	17.88	-0.81
Tap water	W7	1.60	1.52	-0.08

N: No Pb^{2+} was detected

W: waste water

3.7.3. Statistical analysis

In order to verify that the difference in the detection results was caused by the measurement method or other factors, it is necessary to carry out hypothesis testing using a statistical method. As shown in Table 2, seven water samples (W1-W7) were analyzed using the Wilcoxon signed-rank test. The data was processed by the spss20 software, calculated by Z=-1.183, P=0.237, P>0.05 (P<0.05 was considered statistically significant). These results indicated that the differences between the use

of Atomic absorption spectrophotometer (AAS) and the proposed method were no statistically significant, suggesting that there was no difference between the detection results obtained by AAS and by the proposed method were no difference. Thus, the proposed biosensor represented a promising potential for the detection of Pb^{2+} in the environment.

Table 2 Statistical analysis

Sample	Atomic absorption spectrophotometer (nM)	Present work ($\bar{x}$, nM)	Error	Rank
W1	24.70	24.55	-0.15	-5
W2	2.82	2.76	-0.06	-2
W3	6.18	6.06	-0.12	-4
W4	9.35	9.37	0.02	1
W5	12.46	13.15	0.69	6
W6	18.69	17.88	-0.81	-7
W7	1.60	1.52	-0.08	-3
				T_+=7, T_-=21

P>0.05

4. Conclusion

In summary, a selective and sensitive biosensor was developed for monitoring Pb^{2+} in the environmental samples by coupling with a specific DNAzyme modified platform. The use of Pb^{2+}-dependent DNAzyme strengthened the selectivity of the biosensor, whilst utilization of Fe-MOFs/PdPt NPs-HP enhanced the sensitivity for the first time. Compared to the detection performance of conventional Pb^{2+} sensing strategies, the newly designed biosensor showed high sensitivity, good stability, and acceptable reproducibility in Pb^{2+} detection. This method shows a potential for Pb^{2+} determination in naturally contaminated sewage and can be expanded readily for detection of other metal ions in the environment. However, the number of real samples in this study was not large enough, thus the next work is to collect more samples to further prove the feasibility of the biosensor for the detection of Pb^{2+}.

Acknowledgement

We are grateful for the financial support from the National Nature Science Foundation of China (No. 81370403), the Chongqing Foundation and Advanced Research Project (No. CSTC2015jcyjBX0053), the Chongqing Medical University Scientific Research Cultivating Fund(No.201414) and the Outstanding Graduate Student Cultivation Program of Chongqing Medical University (No. BJRC201722).

References

Calvo Quintana, J., Arduini, F., Amine, A., van Velzen, K., Palleschi, G., Moscone, D., 2012. Anal Chim Acta 736, 92-99.

Carne, A., Carbonell, C., Imaz, I., Maspoch, D., 2011. Chem Soc Rev 40, 291-305.

Chen, K. J., Lee, C. F., Rick, J., Wang, S. H., Liu, C. C., Hwang, B. J., 2012. Biosens Bioelectron 33, 75-81.

Fan, T., Liu, Y., Feng, B., Zeng, G., Yang, C., Zhou, M., Zhou, H., Tan, Z., Wang, X., 2008. J Hazard Mater 160, 655-661.

Ge, Y., Wu, J., Ju, H., Wu, S., 2014. Talanta 120, 218-223.

Huang, D. L., Zeng, G. M., Feng, C. L., Hu, S., Jiang, X. Y., Tang, L., Su, F. F., Zhang, Y., Zeng, W., Liu, H. L., 2008. Environ Sci Technol 42, 4946-4951.

Hung, Y. L., Hsiung, T. M., Chen, Y. Y., Huang, C. C., 2010. Talanta 82, 516-522.

Lee, S. J., Anandan, V., Zhang, G., 2008. Biosens Bioelectron 23, 1117-1124.

Li, T., Wang, E., Dong, S., 2010. Anal Chem 82, 1515-1520.

Liang, P., Sang, H., 2008. Anal Biochem 380, 21-25.

Liu, N., Wang, Z., Ma, Z., 2014. Bioanalysis 6, 903-905.

Liu, Y. L., Zhao, X. J., Yang, X. X., Li, Y. F., 2013. Analyst 138, 4526-4531.

Marbella, L., Serli-Mitasev, B., Basu, P., 2009. Angew Chem Int Ed Engl 48, 3996-3998.

Santoro, S. W., Joyce, G. F., 1998. Biochemistry 37, 13330-13342.

Shen, L., Chen, Z., Li, Y., He, S., Xie, S., Xu, X., Liang, Z., Meng, X., Li, Q., Zhu, Z., Li, M., Le, X. C., Shao, Y., 2008. Anal Chem 80, 6323-6328.

Tang, L., Zeng, G. M., Shen, G. L., Li, Y. P., Zhang, Y., Huang, D. L., 2008. Environ Sci Technol 42, 1207-1212.

Tang, S., Tong, P., Li, H., Tang, J., Zhang, L., 2013. Biosens Bioelectron 42, 608-611.

Xie, S., Ye, J., Yuan, Y., Chai, Y., Yuan, R., 2015. Nanoscale 7, 18232-18238.

Xu, H., Xu, P., Gao, S., Zhang, S., Zhao, X., Fan, C., Zuo, X., 2013. Biosens Bioelectron 47, 520-523.

Yuan, G., Yu, C., Xia, C., Gao, L., Xu, W., Li, W., He, J., 2015. Biosens Bioelectron 72, 237-246.

Zhang, C., Lai, C., Zeng, G., Huang, D., Tang, L., Yang, C., Zhou, Y., Qin, L., Cheng, M., 2016. Biosens Bioelectron 81, 61-67.

Highlights

1. Fe-MOFs/PdPt NPs composite was first used for signal amplification to fabricate a highly sensitive biosensor for detecting Pb^{2+}.
2. The high selectivity of the biosensor was achieved by 8–17 DNAzyme cleavage-induced template.
3. The biosensor was applied for detecting Pb^{2+} in real water samples, showing a promising potential for the detection of Pb^{2+} in the environmental.